Semiquantitative Determination of Thiocyanate in Saliva Through Colorimetric Assays: Design of CNN Architecture via Input-Aware NAS

Tommaso Taccioli, Edoardo Ragusa, *Member, IEEE*, Tania Pomili, Paolo Gastaldo, and Pier Paolo Pompa

***Abstract*—This article presents a novel method enabling point-of-care (POC) testing of thiocyanate concentration in saliva. Thiocyanate is an important biological marker; its levels are linked with diseases such as cancer and neurodegeneration. Hence, monitoring this marker frequently can positively impact users' lives. In the proposed setup, the goal is a semiquantitative reading of thiocyanate concentration from colorimetric assays in solution; the user-friendly, yet accurate readout procedure relies on a smartphone camera and is designed to be robust against moderate changes in indoor lighting conditions. The readout procedure exploits the capabilities of convolutional neural networks (CNNs) to fully profit from a setup involving a custom color chart and the assay vial. Thus, a data-driven strategy is adopted to deal with color distortions caused both by lighting conditions and by postprocessing operations embedded in the smartphone camera. A neural architecture search (NAS) procedure explicitly tuned for the problem at hand drove the design of the custom CNN architecture. The method has been tested using a collection of real-world data and compared with existing approaches. The results presented in this article show an increase in accuracy up to about 14% with respect to state-of-the-art methods.**

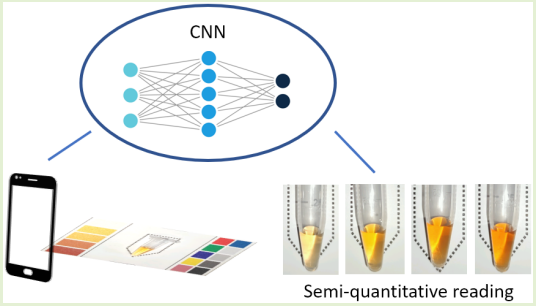

***Index Terms*— Colorimetric test, convolutional neural networks (CNNs), neural architecture search (NAS), point-of-care (POC), saliva, smart sensor.**

I. Introduction

A BIOLOGICAL marker (*biomarker*) is "any substance, structure, or process that can be measured in the body or its products and influence or predict the incidence of outcome or disease" [1]. Thiocyanate is an important biomarker that strongly correlates with a person's well-being: its levels are linked with diseases such as certain types of cancers, atherosclerosis, and neurodegeneration [2], [3], [4], [5], [6] as well as with bacterial infections and tobacco smoke exposure [7], [8], [9], [10]. Monitoring this biomarker frequently can positively impact users' lives, but many technological challenges have to be overcome to develop a fast and easy-to-use point-of-care (POC) sensing device. In fact, although thiocyanate can be sampled noninvasively from saliva, most techniques to assess its concentration require special instrumentation and knowledge, raising issues about costs, assay portability, or ambient conditions stability in the case of instrument-free devices [11].

This article focuses on the semiquantitative reading of thiocyanate concentration in saliva from colorimetric assays in solution [7]. The target is to develop an automatic readout procedure that is robust against moderate changes in indoor lighting conditions. The adopted setup relies on a smartphone camera and a custom color chart that appears beyond the assay vial when the picture is grabbed in indoor settings. Such an approach may lead to an easy-to-use POC device: the user takes a picture of a test with the smartphone and then automatically receives the result on the smartphone display. It is known from the literature that smartphones can serve as cheap and portable readout systems for POC design [12], [13], [14], [15]; this, in turn, leads to inexpensive and fast solutions, which can be used even by untrained users. However, the interpretation of colorimetric test kits is challenging, even in

Manuscript received 7 September 2023; revised 10 October 2023; accepted 10 October 2023. Date of publication 24 October 2023; date of current version 30 November 2023. The associate editor coordinating the review of this article and approving it for publication was Dr. Theerawit Wilaiprasitporn. *(Corresponding author: Edoardo Ragusa.)*

This work involved human subjects or animals in its research. Approval of all ethical and experimental procedures and protocols was granted by the Ethical Committee of Regione Liguria under Application No. 405/2020-DB id 10787.

Tommaso Taccioli, Tania Pomili, and Pier Paolo Pompa are with the Nanobiointeractions and Nanodiagnostics Laboratory, Istituto Italiano di Tecnologia (IIT), 16163 Genova, Italy.

Edoardo Ragusa and Paolo Gastaldo are with the Department of Electrical, Electronics, Telecommunication Engineering and Naval Architecture (DITEN), University of Genoa, 16145 Genova, Italy (e-mail: edoardo.ragusa@unige.it).

Digital Object Identifier 10.1109/JSEN.2023.3325545

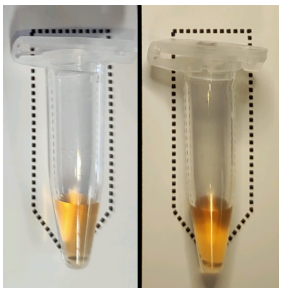

Fig. 1. Same test vial captured under different ambient light conditions. The different illumination strongly impacts the color grade and uniformity as well as the formation of unpredictable shade patterns.

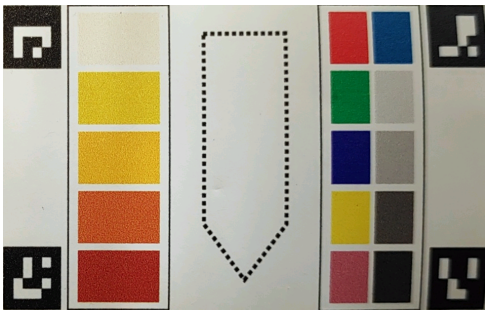

Fig. 2. Custom chart with five reference color patches (on the left of the vial-shaped outline) and ten color correction patches (on the right). The four ArUco markers can be seen on the corners.

the case of commercial products [16], [17], [18]. This process may lead to errors and low accuracy, practically limiting the assays only to those exhibiting strong and distinguishable colors [19]. Hence, the availability of reliable readout procedures can further enhance the features of smartphones as sensing systems.

Recent reviews [20], [21] highlight the lack of robust solutions for the readout of colorimetric analysis in ambient light, as severe limitations affect sensing methods based on smartphone cameras. These issues, in turn, prevent accurate quantitative and semiquantitative colorimetric analyses. Two main issues should be mentioned. First, lighting conditions impact the image captured by the camera. Second, unavoidable low-level, postprocessing operations embedded in the smartphone camera further increase color distortions. Furthermore, assays in solution represent a major problem as the shape and the texture of the vials may produce color gradients, depending on the angle from which the illumination hits the test vial (see Fig. 1).

The main contribution of this article lies in a novel approach based on convolutional neural networks (CNNs) for automated readout of colorimetric assays in solution under ambient light conditions. The proposed approach exploits the effectiveness of CNNs at solving nonlinear problems to fully profit from a setup that involves a custom color chart (Fig. 2) along with the assay vial. Accordingly, the CNN-based model takes advantage of the presence of reference color patches in the captured image to manage color distortions caused both by lighting conditions and postprocessing operations embedded in the smartphone camera. In practice, a data-driven strategy is adopted to bypass explicit color correction techniques, which lack robustness.

A neural architecture search (NAS) procedure automatically generated and evaluated a set of candidate neural network architectures. Such an approach led to a custom CNN designed to tackle the problem at hand: the NAS procedure was specifically designed to select an input-aware architecture, as the candidate networks also differed in the relative weight assigned to each reference color included in the custom chart.

The contribution of the article can be summarized as follows.

1) An automatic readout procedure designed for smartphones that can assess thiocyanate levels in saliva from an assay performed in solution in ambient light.
2) A data-driven procedure to automatically generate and evaluate neural network architectures and optimize the input representation.
3) A NAS search space suitable for colorimetric diagnostic tests performed in solution using smartphone cameras and paper support in ambient light.

Experimental results on real data confirmed the reliability of the proposed approach. The custom CNN architecture yielded from the NAS outperformed state-of-the-art solutions targeting similar problems [22], [23], showing up to a 14.8% increment in accuracy on a ten-class classification problem.

II. Related Works

POC devices have recently attracted a surge in attention in various branches of research and clinical diagnostics [24], [25], [26]. Several types of POCs have been developed for different applications [27], [28], [29], [30] including lab-on-a-chip [31], lab-on-a-disk [32], microfluidic paper-based analytical [33], [34], lateral flow devices [35], [36], and isothermal nucleic acid amplification [37].

Smartphones can effectively support the design of smart POC devices [12], [13], [14], [15]. More specifically, digital cameras [20], [21] play a major role in low-cost sensing as an alternative to spectrophotometric analysis [38], [39]. This, however, is a challenging task mainly due to the instability of the color captured. Existing solutions can be grouped based on physical setup and algorithm.

In some works, enclosures and supports [40], [41] eliminate the detrimental effect on the color of ambient light, using the smartphone flashlight or internal fixed lights as the only illumination source [42], [43]. The presence of external hardware makes these approaches less commercially appealing than operations in ambient light.

Other methods use color correction techniques from computer vision [44], [45]: the setup involves a color board placed close to the assay. A color correction matrix (CCM) maps each pixel to its "true" color. CCM can be obtained using different algorithms: linear color correction, polynomial color correction, and root-polynomial color correction. As stated in [46] and [47], the latter provides the best and most consistent results. However, these methods require the color board and the test to be hit by the same, constant lighting. Moreover, the individual colors of the board should not be saturated, which makes them prone to user errors.

Machine learning (ML) can learn the interaction between light and the assay automatically from data. Most ML methods deal with the fluctuations of ambient light by using reference color charts, which can be put close [48], [49] or farther [22] from the assay. These colors are similar to those appearing in the test and are expected to be affected by light conditions coherently. Flaucher et al. [22] used three different approaches to compare the test and ground-truth colors: Hue value comparison, matching factor, and Euclidean distance, with the last two algorithms computed in the HSV color space.

Among ML techniques, DNNs excel in image processing [23], [50], [51]. In [23], a CNN classified albumin concentration values in urine from a paper-based assay using different smartphones' cameras, evaluating also the performance improvement gained using the smartphones' flash. This method, however, does not provide any additional information to the neural network about the lighting in which the test is taken, with an impact on the overall accuracy.

III. Methodology

This section presents the method for semiquantitative reading of thiocyanate concentration in saliva using colorimetric assays in solution. The research achieves robustness even in indoor ambient light conditions, where the direction, strength, and color of the lighting may vary significantly.

The approach uses fixed reference colors put close to the assay vial that allows the CNN to estimate the light's properties. A NAS procedure selects automatically a suitable CNN architecture in combination with a set of reference colors.

In the following, Section III-A presents the method, while Section III-B introduces the NAS procedure.

A. CNN Architecture for Semiquantitative Reading of Salivary Thiocyanate Concentration in Ambient Light

Our goal is to read the thiocyanate concentration present in saliva, indicated as T, in (1), from a colorimetric assay in solution. The underlying hypothesis is that the assay reflectance R is related to T [7]

$$T = g(R). \tag{1}$$

The smartphone camera provides information about R. In general, cameras perceive colors as a function of the spectrum of the source of light L which strikes a certain dark object and its surface reflectance. Given the same reflectance for an object, a sensor perceives its color differently depending on the spectrum of the light hitting it and its sensitivity S. In our case, the liquid state of the assay is an issue, as the perceived color is altered by the direction from where the light hits the vial and by its strength (see Fig. 1).

As a result, the assay color perceived by the camera C_P is

$$C_P = f(R, L, S). \tag{2}$$

Equation (2) clarifies that to properly assess R, one should know L and S in addition to C_P. Accordingly, estimating T requires solving the inverse problem

$$T = g\big(f^{-1}(C_P, L, S)\big). \tag{3}$$

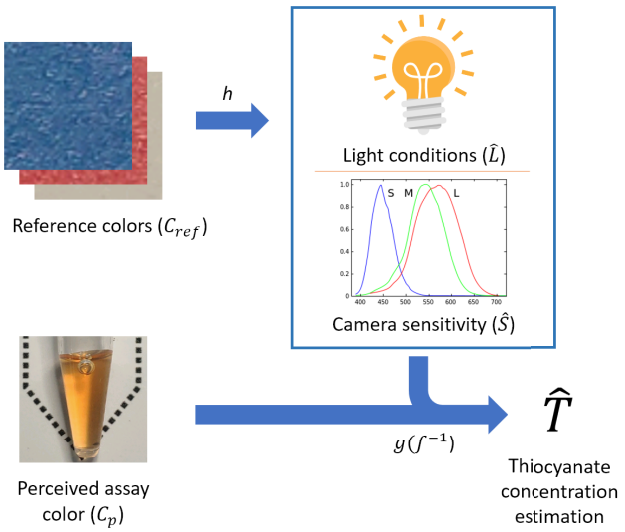

Fig. 3. Theoretical passages needed to retrieve the thiocyanate concentration value from the data obtainable through a picture using our reference color card.

However, both L and S are unknown. The present approach tackles this issue by estimating S and L. Reference colors are placed close to the salivary test by adopting the custom chart of Fig. 2. The chart contains 15 color patches: ten patches have been extracted from popular color correction charts; the remaining five set a reference color scale for the assay with different thiocyanate concentrations. The card contains four ArUco markers [52] on its corners (as per Fig. 2); such markers facilitate the alignment process and the correction process for skewed images, reducing the impact of phone tilt and rotation.

The overall goal is to estimate S and L by using the 15 colors $\{C_{\text{ref},i};\, i = 1, \ldots, 15\}$ captured by the camera. Fig. 3 schematizes the setup. A function h, shown in (4), estimates S and L using the true reflectance value of the reference colors (upper part of Fig. 3)

$$\hat{S}, \hat{L} = h(\{C_{\text{ref}}\}). \tag{4}$$

Then, $\hat{L}$ and $\hat{S}$ are exploited in the solution of the inverse problem (3)

$$\hat{T} = g\big(f^{-1}(C_P, \hat{L}, \hat{S})\big). \tag{5}$$

In the proposed approach, a CNN tackles the problem (5) because an explicit implementation of (5) represents a challenging task due to the multiple sources of noise. Indeed, mathematical approaches [45], [53] may fail to accurately model color representation. CNNs can process both the vial and color patches solving strongly nonlinear problems discerning relevant features inside images and can cope with the refraction and bubbles occurring inside the vial.

In practice, CNNs can learn (5) if trained properly with a dataset collecting images of the vial along with the reference patches. Our CNN processes a cropped image of the vial, together with a crop of the central part of all the color patches which are resized to the same size as the image of the vial, as shown in Fig. 4. The figure shows the proposed CNN meta-architecture. The network processes two inputs

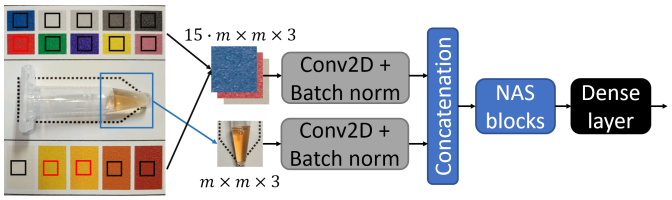

Fig. 4. CNN inputs are obtained by cropping the image. In the scheme of the CNN, NAS Blocks and Conv2D+ Batch norm refer to the part of the architecture obtained through the NAS procedure.

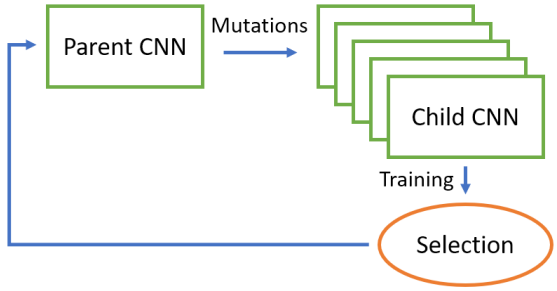

Fig. 5. Block scheme of the evolutionary algorithm used.

separately; each one passes through a convolutional layer and batch normalization layer. Then, a concatenation layer merges the information. The proposed structure prevents a strong bond between the more informative image of the vial and the images of color patches. The NAS procedure generates a single-branch architecture that processes the information from the two input branches. The network's output is the classification of the thiocyanate concentration level.

B. NAS With Input Selection

A blockwise NAS procedure selects the network architecture. Following a standard schema, three components characterized the procedure: the search space, the search algorithm, and the evaluation criteria.

1) Search Space: The search space $\mathbf{S_s}$ collects the candidate network architectures. In the present work, a candidate architecture is a stack of building blocks made of one convolutional layer and one batch normalization layer. The blocks embed three different parameters: the kernel size, the number of filters for each block, and the stride size. Together with the blocks' parameters, the search procedure tunes the number of blocks, the input size, and the color space used for the input images. Eventually, the combination of color patches is integrated into the network architecture to enhance the procedure.

2) Evaluation Criteria: The importance of each color reference is not known a priori. The NAS procedure measures it by generating networks that differ in weights assigned to the patches. The accuracy of the validation set drives the selection.

3) Search Algorithm: The search space is rather vast (or better, infinite). The evolutionary algorithm of Fig. 5 implements the exploration procedure. It generates a set of N "child" architectures starting from a "parent" network by applying random alterations to its structure. The alteration could change the set of reference patches. A parent yields seven different child networks by changing the number of blocks inside it, the three parameters describing the blocks, the color space used for the input images, their size, and which color patches are used. The child with the best evaluation score becomes the new parent, and a new "offspring" will be generated from it. This search strategy allows a wide exploration of the search space with a simple implementation algorithm. Other strategies could tradeoff differently search time and quality of the solution [54], [55], however, a recent comparison suggested that the performance of the solution is similar for different approaches [56].

The procedure is summarized in Algorithm 1, with the following notation: the reference color space $\mathbf{A_s}$ contains all possible permutations of the reference colors $\mathbf{A}$; $\mathbf{CNN_P}$ indicates the parent architecture; $\mathbf{CNN_C}(\mathbf{S_C}, \mathbf{A_C}) = \mathbf{R_m}(\mathbf{CNN_P}(\mathbf{S_P}, \mathbf{A_P}))$ denotes the child architecture generator function; $\mathbf{N_c}$ is the number of child architectures for each of the $\mathbf{N_g}$ generations; finally, $\mathbf{E}(\mathbf{CNN}, \mathcal{X}_\mathcal{V})$ is the evaluation function. After the initialization stage, the procedure generates the first parent architecture (line 1). For a preset number of iterations N_g, the approach generates and train child networks (lines 4 and 6, respectively). Then, the offspring are evaluated and the best one replaces the parent architecture (line 8).

Algorithm 1 Evolutionary NAS With Input Selection

Dataset Training set $\mathcal{X}_\mathcal{T} = \{\mathbf{X_i}, \mathbf{A_i}, \mathbf{Yi}\}_{\mathbf{i=1,\ldots,n}}$ with $\mathbf{X_i}$ assay image, $\mathbf{A_i}$ reference color images, and $\mathbf{Y_i}$ the corresponding thiocyanate concentration class. Validation set $\mathcal{X}_\mathcal{V} = \{\mathbf{X_i}, \mathbf{A_i}, \mathbf{Yi}\}_{\mathbf{i=1,\ldots,m}}$.

Pseudocode

1: **0. Init**: $\mathbf{CNN_P}(\mathbf{S_P}, \mathbf{A_P}) = \mathbf{CNN_{P_0}}(\mathbf{S_{P_0}}, \mathbf{A_{P_0}})$
2: **for g** in $\mathbf{N_g}$ **do**
3: **for c** in $\mathbf{N_c}$ **do**
4: **1. Mutation**: $\mathbf{CNN_{C_c}}(\mathbf{S_{C_c}}, \mathbf{A_{C_c}}) =$
5: $\mathbf{R_m}(\mathbf{CNN_P}, \mathbf{A_P})$
6: **2. Training**: Train $\mathbf{CNN_{C_c}}(\mathbf{S_{C_c}}, \mathbf{A_{C_c}})$ on $\mathcal{X}_\mathcal{T}$
7: **end for**
8: **3. Selection**: $\mathbf{CNN_P}(\mathbf{S_P}, \mathbf{A_P}) =$
9: $\mathbf{argmax}(\mathbf{E}(\{\mathbf{CNN_C}(\mathbf{S_C}, \mathbf{A_C})\}_{\mathbf{j=1,\ldots,N_c}}, \mathcal{X}_\mathcal{V})$
10: **end for**

IV. Experiments

The section is organized as follows. Section IV-A presents the dataset and the experimental setup. Section IV-B reviews the experiments about the NAS procedure. Finally, Section IV-C compares the CNN architecture selected by NAS against two state-of-the-art methods developed to read semiquantitative and binary colorimetric assays performed on paper.

A. Experimental Setup

The experimental setup validates the robustness against moderate variation in lighting conditions when acquiring the results of the colorimetric assay using a smartphone in an indoor environment. The adopted protocol was inspired by the setup proposed in [57] and [23].

The images were collected in a laboratory with fixed lighting conditions (4000 K) without direct interaction with sunlight or other lighting sources. A lamp with three different light temperatures, corresponding to 3000, 4500, and 6000 K, was headed toward the vial changing its orientation and height

TABLE I
DATA SPLIT BETWEEN TRAINING, VALIDATION, AND TESTING SETS WITH THE SMARTPHONE FLASH OFF AND ON

Dataset	*Flash off*	*Flash on*
Training set	2.730	1.942
Validation set	1.226	956
Testing set	518	1.066
Total	4.474	3.964

to mimic real-world conditions. Different orientations induced shadow changes that distorted the color quantification process. Illumination intensities were measured using the light sensors equipped by the smartphone used to capture the pictures. The base illumination was 230 lux. The smallest illumination increment induced by the auxiliary lamp at the highest distance and the steepest inclination was 640 lux. The largest increment was 1725 lux. For each light condition and direction, a set of approximately 20 images was captured while moving the phone around to simulate an average user who could fail in aligning the smartphone with the test tube creating interaction with shadows produced by the vial.

Saliva from seven different healthy donors was collected over four weeks. To simulate a wide range of nonphysiological thiocyanate concentrations and to assess the smartphone-based semiquantitative detection performance, saliva samples were spiked with different biomarker concentrations, so to mimic ten levels of thiocyanate, covering the 0–2.50-mM range uniformly [3], [7], leading to a ten-class problem where each class corresponded to a different concentration level.

All images were captured by a Xiaomi 11 Lite 5G NE phone main camera. The experimental dataset contained 8.438 images, of which 4.474 were acquired with the flash switched off and 3.964 with the flash on. Table I shows the split between training, validation, and testing. Different sets of images included only images of vials with saliva acquired at different times and/or from different persons preventing possible overfitting on irrelevant saliva characteristics (e.g., the presence of bubbles or cloudiness inside the vial).

B. Definition of the CNN Architecture Through NAS Procedure

The initial parent architecture had a basic structure: the concatenation layer was directly linked with the dense layer. The input image size was 80 × 80 pixels, all the color patches shared the same weights, and the adopted color space was RGB. The kernel size, the stride size, and the number of filters for the first convolution were set to 1, 1, and 4, respectively. Each architecture was trained for 100 epochs with the Adam optimizer, categorical cross-entropy loss, and a learning rate of 10^{-3} using early stopping on the validation set with a patience value of 4 epochs. The number of generations $\mathbf{N_g}$ was 100. For each generation, only the child which presented the lowest validation loss was selected. Keras and TensorFlow Python libraries supported the NAS procedure implementation.

The architecture generated from the NAS procedure had an input size of 110 × 110 pixels in LAB color space and two blocks after the concatenation layer. Table II presents the architecture. Each row refers to network blocks composed of one convolutional layer and one batch normalization layer. The first column gives the input size for the corresponding block, while the other columns refer to, respectively, the number of filters, the kernel size, and the stride size of the convolutional layer inside the block. The first row of Table II shows the input of the network composed by the vial image, of size 110 × 110 pixels, and 12 × 3 channels dedicated to the color patches. The NAS procedure eventually selected 12 color patches out of 15; the discarded patches are marked with red squares in Fig. 4. This experiment confirmed the benefits of using these additional inputs to the neural network.

TABLE II
NET ARCHITECTURE YIELDED FROM THE NAS PROCEDURE

Input	*# Filters*	*Kernel size*	*Stride size*
$110^2 \times 3 + 110^2 \times 36$	14	1×1	2×2
$55^2 \times 28$	18	1×1	3×3
$19^2 \times 18$	22	1×1	3×3

In total, the architecture involved 1.928 parameters and required 3.982.522 floating-point operations to process an image, making it suitable for deployment on a smartphone.

C. Comparison With the State of the Art

Recent surveys confirm the lack of works targeting the analysis of colorimetric assays in vials using a smartphone in an unconstrained scenario [20], [21]. In fact, the literature also lacks research targeting automatic readout for thiocyanate quantification. However, some recent works tackled similar problems. Two solutions for readout based on smartphone cameras were selected as the baseline. Both methods have been tuned to tackle the problem at hand. The methods were then trained and tested on the exact same set of data used for the proposed approach (as per Section IV-A).

The first baseline [23] is a CNN trained for automated readout of paper-based test strips for urine albumin. In this setup, the flash of the smartphone is exploited to bias the lighting setup, thus avoiding color references. The neural network for this method has been fed with a suitable cropped image of the vial resized to 64 × 64 pixel to enhance the prediction accuracy.

The second baseline [22] is a solution for smartphone-based colorimetric analysis of urine test strips for at-home prenatal care. The original approach uses an object detection network to identify the positions of the test strip and a few color reference pads. The test strip is compared with the reference color; the concentration value is obtained by computing the distance from the reference colors. Given that the focus of the present article is not on detection, the correct patches were manually extracted from the dataset; in other words, the setup considers the ideal case where all patches are correctly detected. The available patches in the left column of the custom card (Fig. 2) set the reference colors. Actually, the central (i.e., third) patch has been removed in this experiment, as empirical evidence suggested that the baseline improved its accuracy with such a setup. As a result, the experiment tackled a four-class classification problem.

The outcomes of the first experiment comparing the baseline [23] with the proposed work are presented in Table III. In this experiment, the flash was turned off. The table gives the

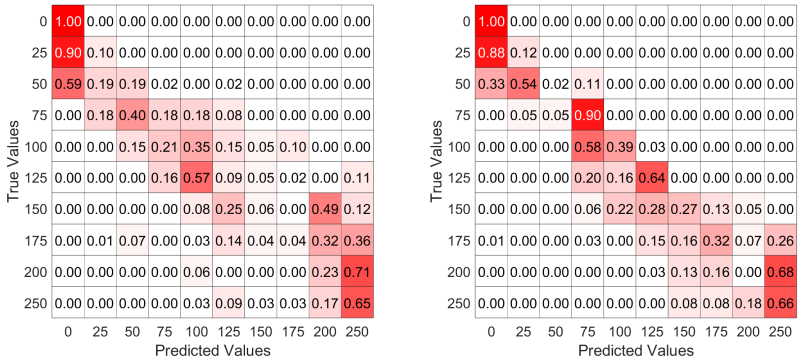

Fig. 6. Confusion matrix on the test set pictures captured with the flash off for the CNN of [23] (left) and the one presented in this article (right).

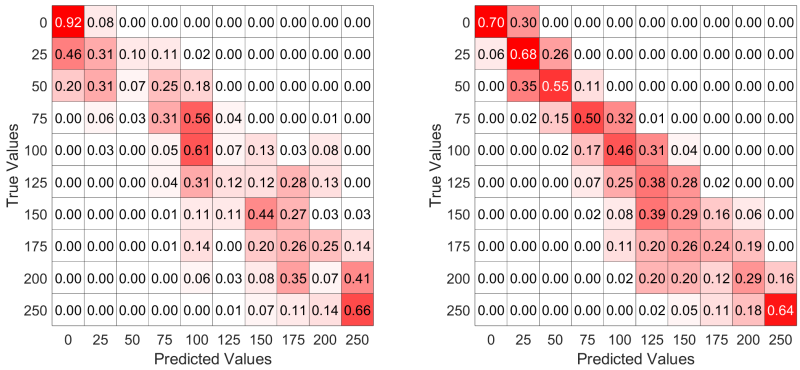

Fig. 7. Confusion matrix on the test set pictures captured with the flash on for the CNN of [23] (left) and the one presented in this article (right).

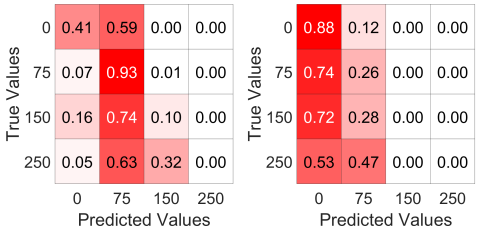

Fig. 8. Confusion matrix on the test set with the flash off (left) and on (right) using the hue distance [22] between the vial and reference color.

TABLE III
ACCURACY COMPARISON OF THE CNN PROPOSED IN [23] AND THE PROPOSAL, COMPUTED ON IMAGES CAPTURED WITH THE FLASH OFF

$Method$	$Accuracy$	$Accuracy+1$
NAS	42.0%	80.9%
$baseline$	27.2%	65.2%

accuracy scored on the test set by, respectively, the CNN selected with the NAS procedure and the CNN proposed in [23]. The column Accuracy + 1 refers to the accuracy obtained when considering acceptable that the *predicted* class is at distance 1 from the *true* class. This metric is reasonable since the basal level of salivary thiocyanate has a certain level of intra- and interpersonal heterogeneity. Accordingly, different samples, belonging to different donors could be affected by a small bias in the original value of thiocyanate. Overall, experimental results show that the proposed approach outperforms the baseline.

Fig. 6 provides the confusion matrices characterizing such an experiment. The matrix on the left side refers to the baseline, while the matrix on the right side refers to the proposal. Each matrix gives all the possible combinations of true labels (rows) and the predicted labels (columns); for each combination, the normalized occurrences are provided. Each box is color-coded depending on its value with a color ranging from white, corresponding to 0, to pure red, corresponding to 1. The confusion matrices suggest that the proposed approach presented a higher accuracy, especially for elevated thiocyanate concentrations, where the assay color produces smaller changes in tone with respect to lower concentrations.

TABLE IV
ACCURACY COMPARISON OF THE CNN PROPOSED IN [23] AND THE PROPOSED CNNS, COMPUTED ON IMAGES CAPTURED WITH THE FLASH ON

$Method$	$Accuracy$	$Accuracy+1$
NAS	46.8%	87.5%
$baseline$	38.1%	78.2%

In the second experiment comparing the baseline [23] with the proposed work, the flash was turned on. Table IV presents the result; it has the same format as Table III. Both methods enhanced their accuracy with respect to the setup with the flash turned off, as suggested in [58] and [23] and the proposal outperformed again the baseline. Fig. 7 shows the confusion matrices obtained with this experiment.

Fig. 8 shows the outcomes of the experiment for the second baseline [22], which exploits as inputs the hue distances between the vial and four reference colors. The figure gives the confusion matrices obtained under two different setups: flash off (left) and flash on (right). In both cases, the baseline proved unsatisfactory, even with a four-class classification problem. In the setup with the flash off, the accuracy was about 39% and worsened with the other setup (about 32%).

V. Conclusion

The article presented a new method for automatic semiquantitative reading of thiocyanate concentration in saliva through assays performed in solution in ambient light. The approach consisted of a convolutional neural network, which exploits information on both the liquid sample and adjacent reference color images. The architecture for the networks was extracted using a NAS able to assert the importance of each reference color. The results confirm the validity of the proposed method, which leads to an acceptable level of accuracy.

References

[1] *Biomarkers in Risk Assessment: Validity and Validation*, World Health Organization, Geneva, Switzerland, 2001.

[2] P. San Gabriel, Y. Liu, A. Schroder, H. Zoellner, and B. Chami, "The role of thiocyanate in modulating myeloperoxidase activity during disease," *Int. J. Mol. Sci.*, vol. 21, no. 17, p. 6450, Sep. 2020.

[3] C. Kalburgi, K. Naik, M. Kokatnur, and S. Warad, "Estimation and correlation of salivary thiocyanate levels in healthy and different forms of tobacco users having chronic periodontitis: A cross-sectional biochemical study," *Contemp. Clin. Dentistry*, vol. 5, no. 2, p. 182, 2014.

[4] Y. Xu, S. Szép, and Z. Lu, "The antioxidant role of thiocyanate in the pathogenesis of cystic fibrosis and other inflammation-related diseases," *Proc. Nat. Acad. Sci. USA*, vol. 106, no. 48, pp. 20515–20519, Dec. 2009.

[5] M. T. Jafari and M. Javaheri, "Selective method based on negative electrospray ionization ion mobility spectrometry for direct analysis of salivary thiocyanate," *Anal. Chem.*, vol. 82, no. 15, pp. 6721–6725, Aug. 2010.

[6] J. Tor-Agbidye, "Bioactivation of cyanide to cyanate in sulfur amino acid deficiency: Relevance to neurological disease in humans subsisting on cassava," *Toxicolog. Sci.*, vol. 50, no. 2, pp. 228–235, Aug. 1999.

[7] F. Pena-Pereira, I. Lavilla, and C. Bendicho, "Paper-based analytical device for instrumental-free detection of thiocyanate in saliva as a biomarker of tobacco smoke exposure," *Talanta*, vol. 147, pp. 390–396, Jan. 2016.

[8] J. D. Chandler and B. J. Day, "THIOCYANATE: A potentially useful therapeutic agent with host defense and antioxidant properties," *Biochem. Pharmacol.*, vol. 84, no. 11, pp. 1381–1387, Dec. 2012.

[9] D. M. Prue, J. E. Martin, and A. S. Hume, "A critical evaluation of thiocyanate as a biochemical index of smoking exposure," *Behav. Therapy*, vol. 11, no. 3, pp. 368–379, Jun. 1980.

[10] E. L. Thomas, T. W. Milligan, R. E. Joyner, and M. M. Jefferson, "Antibacterial activity of hydrogen peroxide and the lactoperoxidase-hydrogen peroxide-thiocyanate system against oral streptococci," *Infection Immunity*, vol. 62, no. 2, pp. 529–535, Feb. 1994.

[11] C. C. Acebal et al., "Application of DV-SIA manifold for determination of thiocyanate ions in human saliva samples," *Talanta*, vol. 96, pp. 107–112, Jul. 2012.

[12] T. Liu, J. Huang, Z. Lin, C. Zhan, D. Yi, and S. Wang, "Multipurpose optical fiber smartphone spectrometer: A point-of-care testing platform for on-site biochemical sensing," *IEEE Sensors J.*, vol. 22, no. 21, pp. 21111–21118, Nov. 2022.

[13] R. Wang et al., "A standalone and portable microfluidic imaging detection system with embedded computing for point-of-care diagnostics," *IEEE Sensors J.*, vol. 22, no. 6, pp. 6116–6123, Mar. 2022.

[14] T. Liu, W. Wang, H. Ding, and D. Yi, "Smartphone-based hand-held optical fiber fluorescence sensor for on-site pH detection," *IEEE Sensors J.*, vol. 19, no. 20, pp. 9441–9446, Oct. 2019.

[15] R. Thakur et al., "Development of smartphone-based lateral flow device for the quantification of LH and E3G hormones," *IEEE Sensors J.*, vol. 20, no. 23, pp. 14491–14500, Dec. 2020.

[16] Macherey-Nagel. *Urine Test Strips Information*. [Online]. Available: https://www.mn-net.com/urine-test-strips-information

[17] Roche. *Combur-Test Strip*. [Online]. Available: https://diagnostics.roche.com/global/en/products/instruments/combur-chemstrip-ins-656.html

[18] D. Hristov, C. Rodriguez-Quijada, J. Gomez-Marquez, and K. Hamad-Schifferli, "Designing paper-based immunoassays for biomedical applications," *Sensors*, vol. 19, no. 3, p. 554, Jan. 2019.

[19] E. Lepowsky, F. Ghaderinezhad, S. Knowlton, and S. Tasoglu, "Paper-based assays for urine analysis," *Biomicrofluidics*, vol. 11, no. 5, Sep. 2017, Art. no. 051501.

[20] Z. Geng, Y. Miao, G. Zhang, and X. Liang, "Colorimetric biosensor based on smartphone: State-of-art," *Sens. Actuators A, Phys.*, vol. 349, Jan. 2023, Art. no. 114056.

[21] K. Fan, W. Liu, Y. Miao, Z. Li, and G. Liu, "Engineering strategies for advancing optical signal outputs in smartphone-enabled point-of-care diagnostics," *Adv. Intell. Syst.*, vol. 5, no. 6, Jun. 2023, Art. no. 2200285.

[22] M. Flaucher et al., "Smartphone-based colorimetric analysis of urine test strips for at-home prenatal care," *IEEE J. Transl. Eng. Health Med.*, vol. 10, pp. 1–9, 2022.

[23] R. Thakur, P. Maheshwari, S. K. Datta, and S. K. Dubey, "Smartphone-based, automated detection of urine albumin using deep learning approach," *Measurement*, vol. 194, May 2022, Art. no. 110948.

[24] Y. Djenouri, A. Belhadi, A. Yazidi, G. Srivastava, P. Chatterjee, and J. C. Lin, "An intelligent collaborative image-sensing system for disease detection," *IEEE Sensors J.*, vol. 23, no. 2, pp. 947–954, Jan. 2023.

[25] M. Tabib-Azar and E. Middleton, "Electronic sensors to detect SARS-CoV-2 viruses in real time," *IEEE Sensors J.*, vol. 23, no. 2, pp. 977–980, Jan. 2023.

[26] S. Nitin Prabhu, C. P. Gooneratne, K.-A. Hoang, and S. C. Mukhopadhyay, "IoT-associated impedimetric biosensing for point-of-care monitoring of kidney health," *IEEE Sensors J.*, vol. 21, no. 13, pp. 14320–14329, Jul. 2021.

[27] C. Wang, M. Liu, Z. Wang, S. Li, Y. Deng, and N. He, "Point-of-care diagnostics for infectious diseases: From methods to devices," *Nano Today*, vol. 37, Apr. 2021, Art. no. 101092.

[28] G. Papadakis et al., "Portable real-time colorimetric LAMP-device for rapid quantitative detection of nucleic acids in crude samples," *Sci. Rep.*, vol. 12, no. 1, pp. 1–15, Mar. 2022.

[29] V. Mastronardi, M. Moglianetti, E. Ragusa, R. Zunino, and P. P. Pompa, "From a chemotherapeutic drug to a high-performance nanocatalyst: A fast colorimetric test for cisplatin detection at ppb level," *Biosensors*, vol. 12, no. 6, p. 375, May 2022.

[30] P. Cecere et al., "Colorimetric point-of-care detection of clostridium tyrobutyricum spores in milk samples," *Biosensors*, vol. 11, no. 9, p. 293, Aug. 2021.

[31] S. Wang, N. Liu, L. Zheng, G. Cai, and J. Lin, "A lab-on-chip device for the sample-in-result-out detection of viable Salmonella using loop-mediated isothermal amplification and real-time turbidity monitoring," *Lab Chip*, vol. 20, no. 13, pp. 2296–2305, 2020.

[32] V. Kordzadeh-Kermani, M. Madadelahi, S. N. Ashrafizadeh, L. Kulinsky, S. O. Martinez-Chapa, and M. J. Madou, "Electrified lab on disc systems: A comprehensive review on electrokinetic applications," *Biosensors Bioelectron.*, vol. 214, Oct. 2022, Art. no. 114381.

[33] T. Pomili, P. Donati, and P. P. Pompa, "Paper-based multiplexed colorimetric device for the simultaneous detection of salivary biomarkers," *Biosensors*, vol. 11, no. 11, p. 443, Nov. 2021.

[34] A. K. Yetisen, M. S. Akram, and C. R. Lowe, "Based microfluidic point-of-care diagnostic devices," *Lab Chip*, vol. 13, no. 12, pp. 2210–2251, 2013.

[35] A. Scarsi, D. Pedone, and P. P. Pompa, "A dual-color plasmonic immunosensor for salivary cortisol measurement," *Nanosc. Adv.*, vol. 5, no. 2, pp. 329–336, 2023.

[36] P. Donati, T. Pomili, L. Boselli, and P. P. Pompa, "Colorimetric nanoplasmonics to spot hyperglycemia from saliva," *Frontiers Bioeng. Biotechnol.*, vol. 8, Dec. 2020, Art. no. 601216.

[37] I. Choopara et al., "Fluorometric paper-based, loop-mediated isothermal amplification devices for quantitative point-of-care detection of methicillin-resistant *Staphylococcus aureus* (MRSA)," *ACS Sensors*, vol. 6, no. 3, pp. 742–751, Mar. 2021.

[38] F. Cai, W. Lu, W. Shi, and S. He, "A mobile device-based imaging spectrometer for environmental monitoring by attaching a lightweight small module to a commercial digital camera," *Sci. Rep.*, vol. 7, no. 1, pp. 1–9, Nov. 2017.

[39] X. Yao, F. Cai, P. Zhu, H. Fang, J. Li, and S. He, "Non-invasive and rapid pH monitoring for meat quality assessment using a low-cost portable hyperspectral scanner," *Meat Sci.*, vol. 152, pp. 73–80, Jun. 2019.

[40] H.-A. Joung et al., "Point-of-care serodiagnostic test for early-stage lyme disease using a multiplexed paper-based immunoassay and machine learning," *ACS Nano*, vol. 14, no. 1, pp. 229–240, Jan. 2020.

[41] E. Ragusa, R. Zunino, V. Mastronardi, M. Moglianetti, P. P. Pompa, and P. Gastaldo, "Design of a quantitative readout in a point-of-care device for cisplatin detection," *IEEE Sensors Lett.*, vol. 6, no. 11, pp. 1–4, Nov. 2022.

[42] M. Wirth et al., "A prospective observational pilot study to test the feasibility of a smartphone enabled uChek urinalysis device to detect biomarkers in urine indicative of preeclampsia/eclampsia," *Health Technol.*, vol. 9, no. 1, pp. 31–36, Jan. 2019.

[43] E. Ragusa et al., "Random weights neural network for low-cost readout of colorimetric reactions: Accurate detection of antioxidant levels," in *Proc. Int. Conf. Syst.-Integr. Intell.* Cham, Switzerland: Springer, 2023, pp. 95–104.

[44] S. H. de Cortina et al., "Laboratory evaluation of a smartphone-based electronic reader of rapid dual point-of-care tests for antibodies to human immunodeficiency virus and treponema pallidum infections," *Sexually Transmitted Diseases*, vol. 44, no. 7, pp. 412–416, 2017.

[45] M. N. Sakinah and A. H. Saputro, "Color correction technique using an artificial color board and root-polynomial color correction for smartphone-based urinalysis," in *Proc. 17th Int. Conf. Quality Res. (QIR), Int. Symp. Electr. Comput. Eng.*, Oct. 2021, pp. 21–26.

[46] J. Sui et al., "Tongue image color correction method based on root polynomial regression," in *Proc. IEEE 8th Joint Int. Inf. Technol. Artif. Intell. Conf. (ITAIC)*, May 2019, pp. 1337–1342.

[47] H. Gong and G. Finlayson, "Root-polynomial color homography color correction," Univ. East Anglia, Norwich, U.K., Tech. Rep., 2017.

[48] S.-H. Han, M.-S. Ra, G.-S. Lee, W.-Y. Kim, and D.-A. Kim, "A novel design of urine test strip with spatially adjacent reference color chart," in *Proc. 18th IEEE Int. Symp. Consum. Electron. (ISCE)*, Jun. 2014, pp. 1–2.

[49] M. Ra, M. S. Muhammad, C. Lim, S. Han, C. Jung, and W.-Y. Kim, "Smartphone-based point-of-care urinalysis under variable illumination," *IEEE J. Transl. Eng. Health Med.*, vol. 6, pp. 1–11, 2018.

[50] N. Bang-iam, Y. Udnan, and P. Masawat, "Design and fabrication of artificial neural network-digital image-based colorimeter for protein assay in natural rubber latex and medical latex gloves," *Microchem. J.*, vol. 106, pp. 270–275, Jan. 2013.

[51] R. Fisher, K. Anderson, and J. B. Christen, "Using machine learning to objectively determine colorimetric assay results from cell phone photos taken under ambient lighting," in *Proc. IEEE Int. Midwest Symp. Circuits Syst. (MWSCAS)*, Aug. 2021, pp. 467–470.

[52] S. Garrido-Jurado, R. Muñoz-Salinas, F. J. Madrid-Cuevas, and R. Medina-Carnicer, "Generation of fiducial marker dictionaries using mixed integer linear programming," *Pattern Recognit.*, vol. 51, pp. 481–491, Mar. 2016.

[53] H. Karlsen and T. Dong, "A smart phone-based robust correction algorithm for the colorimetric detection of urinary tract infection," in *Proc. 37th Annu. Int. Conf. IEEE Eng. Med. Biol. Soc. (EMBC)*, Aug. 2015, pp. 1251–1254.

[54] T. Elsken, J.-H. Metzen, and F. Hutter, "Simple and efficient architecture search for convolutional neural networks," 2017, *arXiv:1711.04528*.

[55] B. Baker, O. Gupta, N. Naik, and R. Raskar, "Designing neural network architectures using reinforcement learning," 2016, *arXiv:1611.02167*.

[56] Y. Liu, Y. Sun, B. Xue, M. Zhang, G. G. Yen, and K. C. Tan, "A survey on evolutionary neural architecture search," *IEEE Trans. Neural Netw. Learn. Syst.*, vol. 34, no. 2, pp. 550–570, Feb. 2023.

[57] A. Y. Mutlu, V. Kılıç, G. K. Özdemir, A. Bayram, N. Horzum, and M. E. Solmaz, "Smartphone-based colorimetric detection via machine learning," *Analyst*, vol. 142, no. 13, pp. 2434–2441, 2017.

[58] R. Thakur, P. Maheshwari, S. K. Datta, S. K. Dubey, and C. Shakher, "Machine learning-based rapid diagnostic-test reader for albuminuria using smartphone," *IEEE Sensors J.*, vol. 21, no. 13, pp. 14011–14026, Jul. 2021.

Tommaso Taccioli was born in 1997, Genova, Italy. He received the B.S. and M.S. degrees in electronic engineering from the University of Genoa, Genova, in 2019 and 2022, respectively.

In 2022, he joined the Nanobiointeractions and Nanodiagnostic Laboratories, Istituto Italiano di Tecnologia (IIT), Genova, as a Fellow. Collaborating with the SEA Lab, University of Genoa, he worked on the development of computer vision algorithms and neural networks for smart sensing in POC devices.

Edoardo Ragusa (Member, IEEE) received the master's (cum laude) degree in electronic engineering and the Ph.D. degree in electronic engineering from the University of Genoa, Genova, Italy, in 2015 and 2018, respectively.

He is currently a Researcher with DITEN, University of Genoa, where he teaches digital systems electronics and machine learning. He coauthored more than 45 refereed papers in international journals and conferences. His research interests include machine learning in resource-constrained devices, convolutional neural networks, and deep-learning applications.

Dr. Ragusa was a Technical Program Chair of the conference "System-Integrated Intelligence: Intelligent, Flexible and Connected Systems in Products and Production," Genova, in 2022. He is a reviewer for several IEEE, Springer, and Elsevier journals and conferences. He is contributing as a Guest Editor to *Future Generation Computer Systems* (Elsevier) and *Electronics* Multidisciplinary Digital Publishing Institute (MDPI).

Tania Pomili received the Ph.D. degree in pharmaceutical chemistry and technology from the University of Camerino, Camerino, Italy, in 2019, and the Ph.D. degree from the University of Genoa, Genova, Italy, in March 2023. Her Ph.D. thesis was highly interdisciplinary and focused on the realization of hybrid point-of-care (POC) devices for the detection of biomarkers and drugs in noninvasive fluids.

She is working with the Nanobiointeractions and Nanodiagnostics Laboratories, Istituto Italiano di Tecnologia (IIT), Genova. She is currently joining a postdoctoral research position with the Nanobiointeractions and Nanodiagnostics Laboratories. Her research project deals with the development and validation of smart sensing strategies for POC diagnostics aiming at detecting biomarkers of neurogenerative diseases and wellness, combining naked-eye and smartphone-based reading.

Paolo Gastaldo received the Laurea degree in electronic engineering and the Ph.D. degree in space sciences and engineering from the University of Genoa, Genova, Italy, in 1999 and 2004, respectively.

In 2004, he joined the Department of Biophysical and Electronic Engineering, University of Genoa, where he was a recipient of a Research Grant on Intelligent Systems for Visual Quality Estimation sponsored by Philips Research Laboratories, Eindhoven, The Netherlands. Since 2011, he has been with the Smart Embedded Applications Laboratory (SEALab), Department of Electrical, Electronics, and Telecommunication Engineering and Naval Architecture, DITEN, University of Genoa, where he currently holds the position of an Associate Professor. He coauthored more than 100 refereed papers in international journals and conferences. His main research interests are in the field of embedded machine learning, machine learning for computer vision, embedded systems for advanced signal interpretation in robotics and prosthetics, and intelligent systems for cybersecurity.

Pier Paolo Pompa is a Research Director and the Head of the Nanobiointeractions & Nanodiagnostics Labs, Istituto Italiano di Tecnologia (IIT), Genova, Italy. He is also a Contract Professor with the Department of Biotechnology, University of Genoa, Genova, a member of the Department of Chemistry, University Board for PhD School, an Editorial Board Member of several international journals, and a member of the Scientific Committee of several international conferences. His scientific activities are highly interdisciplinary, ranging from nanotechnology to biophysics, nanodiagnostics, nanomedicine, and nanobiotechnology, and mainly focus on nanobiointeractions and the development of smart sensing strategies for POC diagnostics. He has authored more than 180 peer-reviewed publications (with more than 12 500 citations), several book chapters, and many invited and oral contributions to international conferences. He is also the author of more than 25 international patents. He led various national and international projects in the field of nanobiotechnology (more than 7 M€ of competitive grants).

Open Access funding provided by 'Università degli Studi di Genova' within the CRUI CARE Agreement